

# On the Structure, Transformation and Deformation of Long-Period Stacking Ordered Phases in Mg-Y-Zn Alloys

J.F. NIE, Y.M. ZHU, and A.J. MORTON

Ternary Mg-Y-Zn alloys have attracted considerable attention due to their unique microstructures and promising mechanical properties. The microstructure of these alloys contains predominantly intermetallic phases of 18R and/or 14H long-period stacking ordered (LPSO) structures, depending on the alloy processing conditions. Such 18R and/or 14H structures or similar LPSO structures are also found in other magnesium alloys such as Mg-Gd-Zn, Mg-Gd-Y-Zn, Mg-Dy-Zn, Mg-Ho-Zn, Mg-Er-Zn, Mg-Y-Cu, Mg-Y-Ni, and Mg-Y-Co. In addition, LPSO structures such as 24R and 10H have also been reported, even though they are less frequently observed. This paper provides a review of the current status on the characterization of the structure, thermal stability, transformation, and deformation of the LPSO structures using high-angle annular dark-field scanning transmission electron microscopy and electron diffraction. Unsolved issues on the LPSO structures are also highlighted and discussed.

DOI: 10.1007/s11661-014-2301-6

© The Minerals, Metals & Materials Society and ASM International 2014

## I. INTRODUCTION

LONG-PERIOD stacking-ordered (LPSO) structures in Mg-Y-Zn alloys have received considerable interest in recent years due to their unique crystallographic features and promising mechanical properties. In general, such LPSO phases form in Mg-RE-X systems, where RE represents Y, Gd, Dy, Ho, Er, Tm, and Tb, and X represents Zn, Cu, Ni, or Co.<sup>[1-8]</sup> In most of these systems, the LPSO phase has an 18R structure in the as-cast condition and a 14H structure in the heat-treated condition. LPSO phases with 24R or 10H structures have also been reported, even though they are much less frequently observed in the alloy microstructures. While significant progress has been made over the past 10 years, there are still some controversial issues on the structure, thermal stability, structural transformation, and deformation of the LPSO phases. It is the purpose of the present paper to provide an overview of the crystal structures, transformations, and deformation of the LPSO phases, with the assistance of recent results made from atomic-resolution high-angle annular dark-field scanning transmission electron microscopy (HAADF-STEM). Some unsolved issues that require further research are highlighted and discussed in this overview. We hope that such knowledge will provide the basis for searching for new Mg-based alloy systems that are free of RE elements and still have LPSO phases and for developing magnesium alloys with desirable microstructures for achieving improved mechanical properties.

---

J.F. NIE, Professor, and Y.M. ZHU, Postdoctoral Research Fellow, are with the Department of Materials Engineering, Monash University, Clayton, VIC 3800, Australia. Contact e-mail: Jianfeng.nie@monash.edu  
A.J. MORTON, Honorary Senior Research Fellow, is with the Department of Materials Engineering, Monash University, and also with the CSIRO Process Science and Engineering, Clayton, VIC 3168, Australia.

A.J. Morton has been a retired person, and work covered by this paper was done at Monash.

Manuscript submitted November 8, 2013.

Article published online April 29, 2014

## II. STRUCTURES OF LPSO PHASES

### A. 18R and 14H

Figure 1 shows intermetallic particles of LPSO phases that are typically observed in Mg-Y-Zn alloys. The formation of the LPSO phases in magnesium alloys was first reported by Luo *et al.*<sup>[1]</sup> They reported that the intermetallic particles formed in grain boundaries of their alloy, Mg-7.2 wt pct Y-1.2 wt pct Zn-0.48 wt pct Zr, are X phase and that this X phase has an 18R modulated structure. They further suggested that the 18R modulated structure could be described as a face-centered cubic structure with  $a = 0.45$  nm. While having not mentioned specifically in their paper, they took these intermetallic particles as the equilibrium phase X, with an atomic composition of Mg<sub>12</sub>ZnY, which has been reported to exist in the Mg-Y-Zn system.<sup>[9]</sup> About 6 years later, Luo and Zhang<sup>[10]</sup> provided, in a separate paper, a more detailed characterization and description of the so-called X phase. Based on selected area electron diffraction (SAED) patterns in a  $\langle 11\bar{2}0 \rangle$  zone axis and high-resolution transmission electron microscopy images, they proposed that the 18R has a trigonal structure with  $a = 1.5772$  nm and  $\alpha = 11.73$  deg, or a hexagonal structure with  $a = 0.3224$  nm and  $c = 4.6985$  nm and that the stacking sequence of the close-packed planes of the 18R structure was ABABABCACACABCBCBCA. The proposed stacking sequence had ABCA-type building blocks, even though the authors did not mention this specifically in their paper. It should be noted that the arrangement of these building blocks in the above expression did not reflect the real symmetry of the structure but did reflect the ordered stacking of the close-packed planes.

In 2001, Kawamura *et al.*<sup>[11]</sup> produced an Mg-2 at. pct Y-1 at. pct Zn alloy using combined methods of gas atomization, compaction, and hot extrusion. This alloy exhibited an impressively high 0.2 pct proof strength exceeding 600 MPa and an elongation to

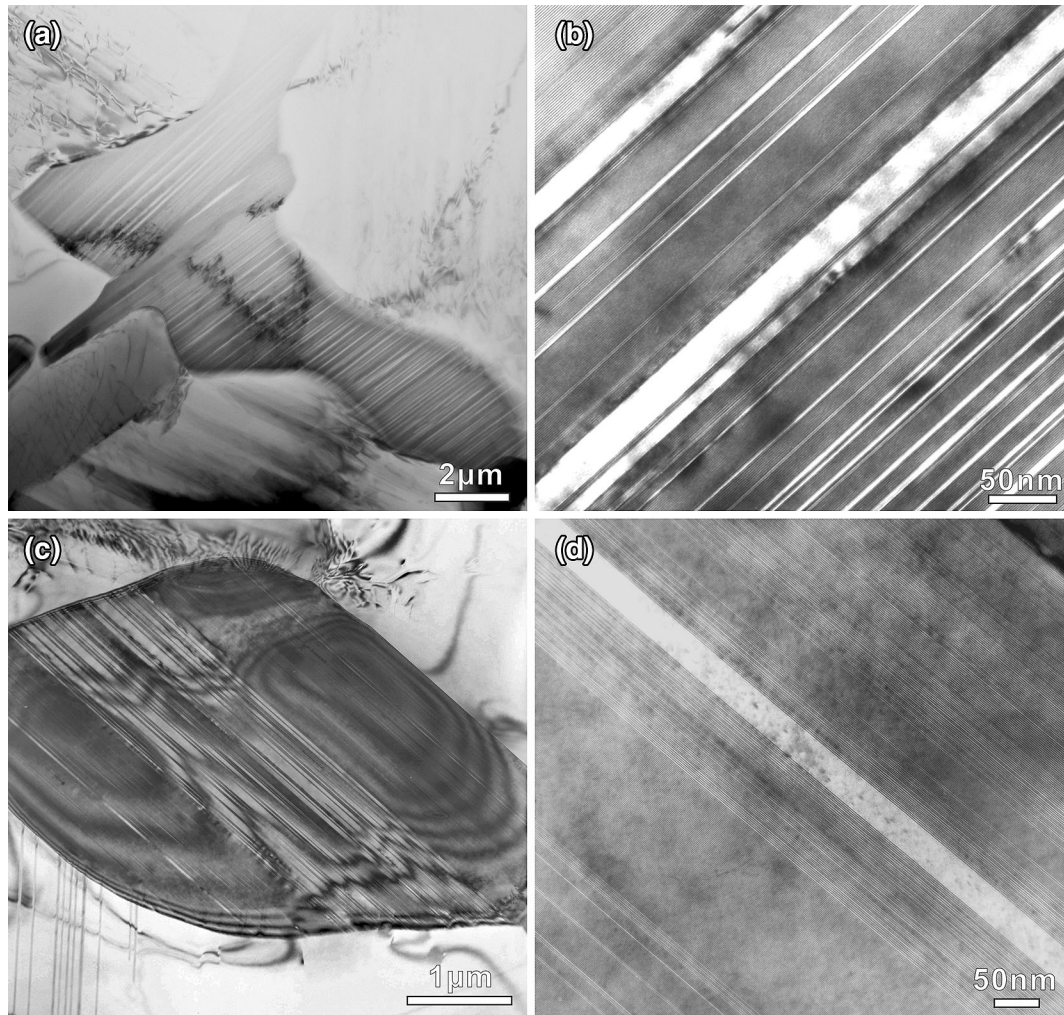


Fig. 1—(a) Bright-field TEM image showing intermetallic particles with LPSO structures in an as-cast sample of the Mg-8Y-2Zn-0.6Zr (wt pct) alloy; (b) enlarged image from a local region of the particle in (a) showing that the distribution of the LPSO structures is not uniform; (c) bright-field TEM image showing an intermetallic particle in a sample of the Mg-8Y-2Zn-0.6Zr (wt pct) alloy heat-treated for 16 h at 773 K (500 °C); (d) enlarged image from a local region of the particle in (c).

fracture of 5 pct.<sup>[11]</sup> The intermetallic particles of the 18R LPSO phase were dispersed in the hot extruded microstructure, and their size was in the range 50 to 250 nm. The studies made in the following years<sup>[12,13]</sup> indicate that this 18R phase can form readily from the melt, irrespective of the solidification rates in the casting, and that this phase can be produced in larger volume fractions when the concentrations of Y and Zn in the Mg-Y-Zn alloy are increased. In the initial study made by HAADF-STEM,<sup>[14]</sup> the intermetallic particles in the Mg-Y-Zn alloys were erroneously suggested to have a 6H structure which has a monoclinic unit cell ( $a = 0.56$  nm,  $b = 0.32$  nm,  $c = 1.56$  nm and  $\beta = 88^\circ$ ) and an ABCBCB' stacking sequence of the close-packed planes. In this proposed 6H structure, the A and B' layers are significantly enriched by Zn and Y, with the Y and Zn content of approximately 10 and 3 at. pct, respectively, in each of these two layers.<sup>[15]</sup> In subsequent studies,<sup>[12,13]</sup> it was recognized that the 6H structure was incorrect and was superseded by the 18R

structure (hexagonal unit cell,  $a = 0.321$  nm,  $c = 4.86$  nm) with an ACBCBCBACACACBABABA stacking sequence of the close-packed planes. This structure is identical to that of the X-Mg<sub>12</sub>YZn phase proposed by Luo and Zhang.<sup>[10]</sup> In all such studies, the term “order” refers to the ordered stacking of the close-packed planes, rather than ordered arrangement of Y and Zn atoms within the close-packed planes.

In 2010, the 18R structure was reported<sup>[16]</sup> to be *ordered* monoclinic ( $a = 1.112$  nm,  $b = 1.926$  nm,  $c = 4.689$  nm, and  $\beta = 83.25^\circ$ ), with Y and Zn atoms occupying some specific positions of the unit cell, Figure 2(a). Note that the c-axis value of the monoclinic unit cell should be 4.722 nm ( $4.689/\sin 83.25$  deg), rather than the proposed 4.689 nm. The orientation relationship between the 18R and  $\alpha$ -Mg phases was such that  $(001)_{18R} // (0001)_\alpha$  and  $[010]_{18R} // \langle 1210 \rangle_\alpha$ . The proposed 18R unit cell has an ABABCACACABCBCBCABA stacking sequence of its close-packed planes and is made up of three building blocks, with adjacent blocks

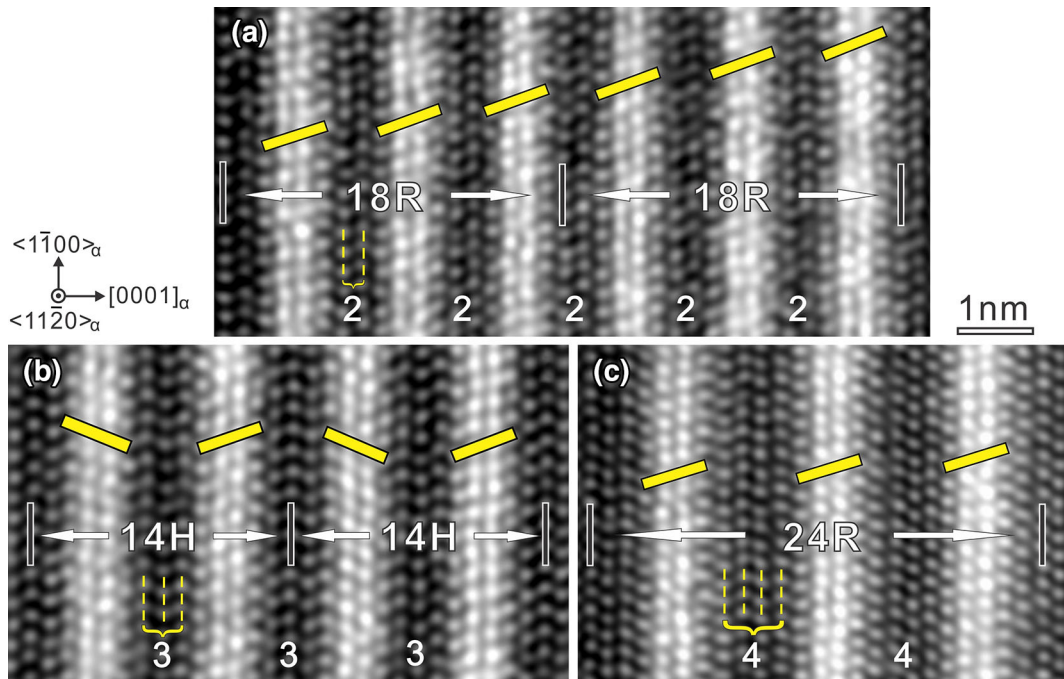


Fig. 2— $\langle 1\bar{1}20 \rangle_x$  HAADF-STEM images showing the characteristic features for the unit cell of (a) 18R, (b) 14H, and (c) 24R. The samples of the Mg-8Y-2Zn-0.6Zr (wt pct) alloy were heat-treated at 773 K (500 °C) for 1 h for (a) and 16 h for (b) and (c).

separated by two  $(0001)_\alpha$  planes of magnesium. Each building block has an ABCA-type stacking sequence, and Y and Zn atoms are concentrated in the B and C layers, resembling closely that of  $\gamma'$  phase formed in Mg-Gd-Zn alloys.<sup>[4]</sup> However, the Y and Zn atoms have an ordered arrangement in the B and C layers, *i.e.*, the two middle layers of each building block in the Mg-Y-Zn alloys. The experimental measurements and this latter model for the 18R structure indicated that its stoichiometric composition is close to Mg<sub>10</sub>YZn, rather than Mg<sub>12</sub>YZn as has long been assumed and commonly accepted in earlier studies. This problem occurred presumably, because the 18R structure was mistakenly taken as the structure of the equilibrium X-Mg<sub>12</sub>YZn phase in the work of Luo and Zhang.<sup>[10]</sup> Luo and Zhang<sup>[10]</sup> did not provide any information on their sample preparation conditions, and it is very likely that the intermetallic particles that they studied are the 18R phase, rather than the equilibrium X-Mg<sub>12</sub>YZn phase.

As described earlier, the 18R phase is observed predominantly in the as-cast microstructure of Mg-Y-Zn alloys. The accumulated experimental evidence from further investigations<sup>[12,13,17–19]</sup> and the calculated Mg-Y-Zn phase diagram<sup>[20,21]</sup> indicate that 18R is not thermodynamically stable at temperatures below 810 K (537 °C) for some Mg-Y-Zn alloy compositions; it is gradually replaced by another type of LPSO, 14H, after prolonged heat treatment at 623 K to 773 K (350 °C to 500 °C).

Initially, it was reported that the 14H structure had a hexagonal lattice ( $a = 0.321$  nm and  $c = 3.694$  nm),<sup>[12]</sup> with its closely packed planes arranged in an ACBCBABABABCBCA stacking sequence. It was subsequently speculated<sup>[4]</sup> that the 14H was made of two building blocks, which was experimentally confirmed in

the following year.<sup>[16,22]</sup> The study<sup>[22]</sup> also indicated that the 14H has, in fact, ordered hexagonal structure ( $a = 1.112$  nm,  $c = 3.647$  nm), and the stacking sequence of the close-packed planes is ABABCACACAC BABA. The 14H unit cell is made up of two building blocks that are separated by three  $(0001)_\alpha$  planes of magnesium, Figure 2(b). It is to be noted that, while the building blocks for the 18R structure are all of the same sign, *i.e.*, ABCA, CAB, and BCAB, the two building blocks within 14H are necessarily of opposite sign, ABCA and ACBA (see discussion below, B). In each building block, the Y and Zn atoms have an *ordered* arrangement in the B and C layers, *i.e.*, the two middle layers. The composition of the 14H structure is Mg<sub>12</sub>YZn (at. pct), identical to that of the equilibrium X phase in the Mg-Y-Zn system.<sup>[1,10]</sup> The orientation relationship between 14H and  $\alpha$ -Mg is that  $(0001)_{14H} // (0001)_\alpha$  and  $\langle 0\bar{1}10 \rangle_{14H} // \langle 1\bar{2}10 \rangle_\alpha$ . The stacking sequence of the close-packed planes of the building block of the 14H and 18R phases is identical to that of the  $\gamma'$  phase in Mg-Gd-Zn alloys,<sup>[4]</sup> even though the  $\gamma'$  phase is disordered.

On the basis of these previous studies, both 18R and 14H are now accepted as being composed of building blocks that have an ABCA-type stacking sequence of its close-packed planes, with the two middle atomic layers rich in Y and Zn.<sup>[22]</sup> However, in very recent studies of LPSO structures in Mg-5 at. pct Gd-3.5 at. pct Al<sup>[23]</sup> and Mg-2 at. pct Y-1 at. pct Zn, Mg-9 at. pct Y-6 at. pct Zn, and Mg-2 at. pct Er-1 at. pct Zn<sup>[24]</sup> alloys, Yokobayashi *et al.*<sup>[23]</sup> and Egusa and Abe<sup>[24]</sup> pointed out that the enrichment of Y and Zn atoms occurred in the consecutive four layers of the ABCA building blocks, with the greatest enrichment occurring

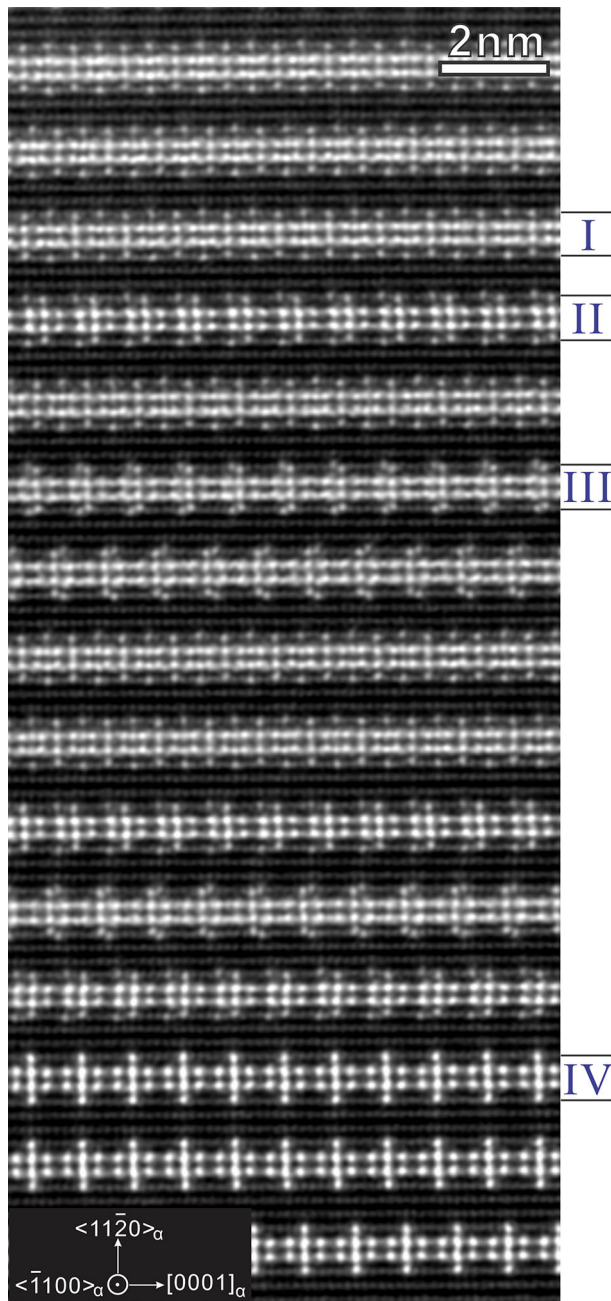


Fig. 3— $\langle 10\bar{1}0 \rangle_z$  HAADF-STEM image showing at least four different types of LPSO structure in an Mg-10Y-1Al (wt pct) alloy heat-treated for 48 h at 823 K (550 °C).

in the inner two layers. For the Mg-Gd-Al alloy, there was evidence that the heavy atoms in the outer layers were strongly ordered leading to a larger unit cell for both the 18R and 14H type “LPSO” phases<sup>[23]</sup> which can also be proved by first-principles calculation.<sup>[25,26]</sup> However, it should be pointed that the SAED patterns recorded from the LPSO phase in this alloy, Figure 2 in Reference 23, are not fully consistent with those obtained from the LPSO phase in the Mg-Y-Zn alloys, Figure 11 in Reference 23. More recently, a range of at least four different LPSO type structural arrangements have been found to exist side by side in an Mg-Y-Al

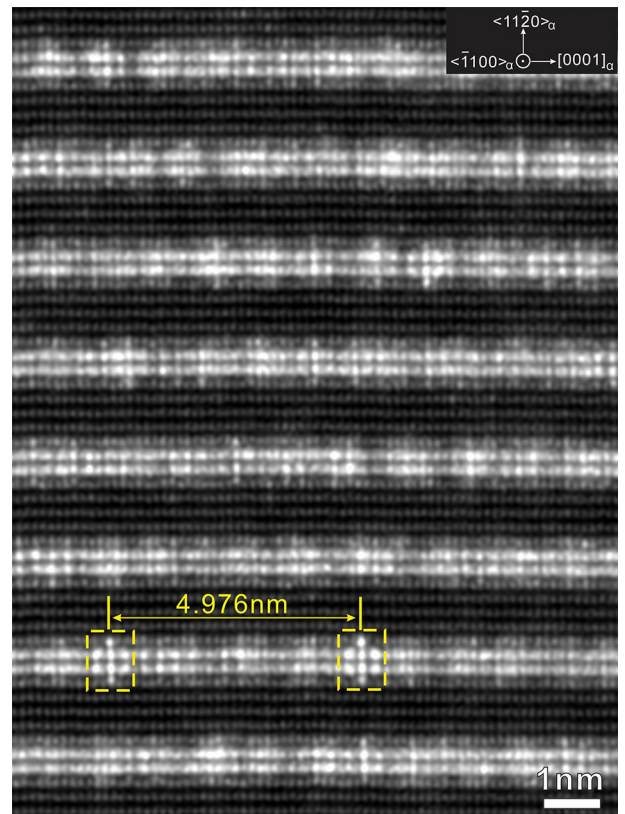


Fig. 4— $\langle 10\bar{1}0 \rangle_z$  HAADF-STEM image showing irregular arrangement of heavy atoms in 14H. The sample of the Mg-8Y-2Zn-0.6Zr (wt pct) alloy was heat-treated at 773 K (500 °C) for 16 h.

alloy, marked as I, II, III, and IV in Figure 3. Hence, further efforts are needed in order to unambiguously establish the structural arrangements in these alloys and whether the range of structures observed for the LPSO phase in the Mg-Gd-Al or Mg-Y-Al alloys is representative of that of the Mg-Y-Zn alloys.

For the Mg-2 at. pct Y-1 at. pct Zn, Mg-9 at. pct Y-6 at. pct Zn, and Mg-2 at. pct Er-1 at. pct Zn alloys,<sup>[24]</sup> there was little evidence of systematic ordering of the heavy atoms on the outer layers. The HAADF-STEM images of the 18R and 14H phases do not show any strong evidence of a systematic ordering of Y and Zn atoms in the two outer layers, and the SAED patterns obtained from the LPSO phases in these three alloys are not fully self-consistent in terms of the intensity of some reflections. As shown in the HAADF-STEM image in Figure 4, some segregation of Y and Zn atoms has occurred in the two outer layers of the ABCA building block. While such distribution of Y and Zn atoms in the ABCA building block resembles that observed in the Mg-Gd-Al alloy, it is not periodic at all along the directions normal and within the close-packed planes. Again, a further systematic study is needed in the future to reconcile the HAADF-STEM images and SAED patterns obtained from different alloys and alloys prepared under different processing conditions, and to establish whether the degree of chemical ordering of the LPSO phases is dependent of the composition and heat treatment conditions of the alloys. With the application

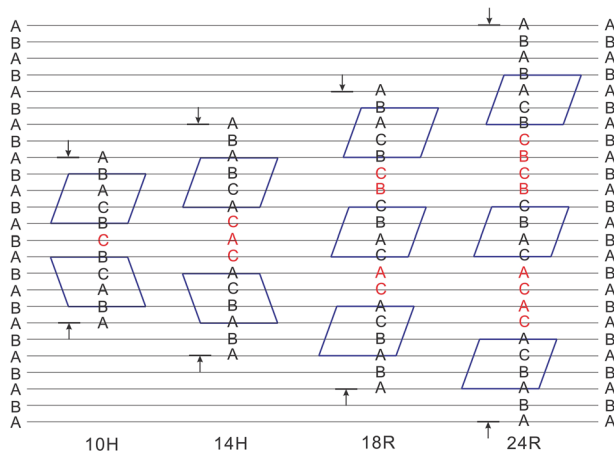


Fig. 5—Schematic diagram showing the characteristic stacking features for the unit cells of the 10H, 18R, 14H, and 24R LPSO structures. The 10H and 14H structures, with an odd number of  $\alpha$ -Mg planes (1 and 3, respectively, as indicated by red color) separating the building blocks necessarily, have opposite stacking sequences in the building blocks, whereas 18R and 24R, with only 2 and 4  $\alpha$ -Mg layers, respectively, separating the building blocks necessarily, have building blocks with the same stacking sequence.

of new electron microscopy techniques, such as atomic-resolution EDS mapping, it will be feasible to precisely define the arrangements of atoms of individual alloying elements such as Y and Zn atoms in LPSO in future studies.

While 18R and 14H are the most frequently observed LPSO structures in Mg-Y-Zn alloys, and many other magnesium alloys such as Mg-Gd-Zn,<sup>[2-4]</sup> Mg-Gd-Y-Zn,<sup>[5]</sup> Mg-Dy-Zn, Mg-Ho-Zn, Mg-Er-Zn,<sup>[6]</sup> Mg-Y-Cu(-Zn),<sup>[7]</sup> Mg-Y-Ni, Mg-Y-Co,<sup>[8]</sup> and possibly Mg-Gd-Al<sup>[23,27]</sup> and Mg-Y-Al, a few other long-period structures such as 10H and 24R have also been reported.<sup>[13,28]</sup> However, whether these LPSO structures are also ordered or not, and their relationships with the ABCA-type building block and 18R and 14H structures remain to be unambiguously established.

### B. 24R and 10H

As we have seen above, the 14H and 18R LPSO structures are based around four-layer building blocks separated by planes of close-packed Mg atoms, three such planes between the building blocks ABCA and ACBA for the 14H structure and just two for the 18R structure in which each building block is of the same type, *i.e.*, all ABCA or all ACBA. The 24R and 10H structures are simply formed by building blocks being separated by four Mg layers (24R), Figure 2(c), and just one Mg layer (10H), respectively. As shown in Figure 5, the number of Mg layers between the building blocks also controls the requirement for the building blocks to be of the same or opposite orientation and hence is a factor in determining the symmetry of the unit cell. In 10H and 14H, with one and three Mg basal plane layers between the building blocks, the building blocks have opposite orientations, whereas 18R and 24R each have three building blocks of the same orientation separated by two and four Mg basal plane layers, respectively.

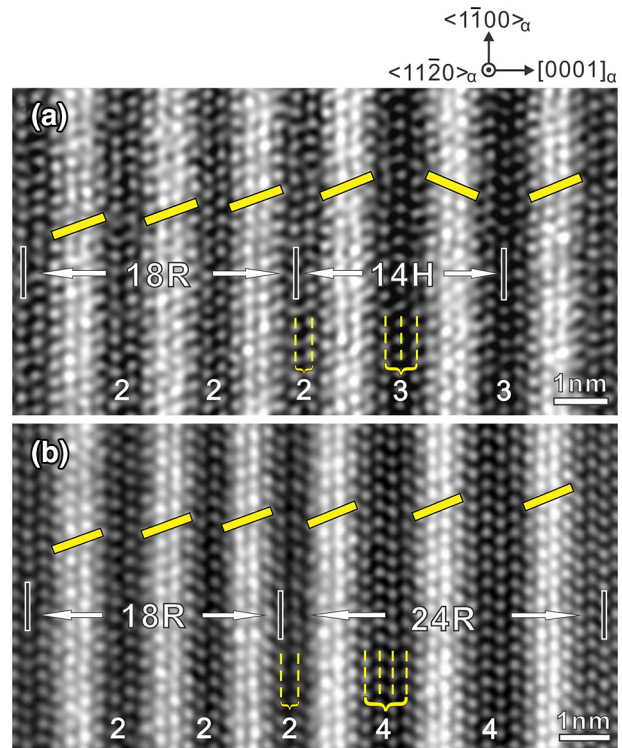


Fig. 6— $\langle 11\bar{2}0 \rangle_\alpha$  HAADF-STEM images in the Mg-8Y-2Zn-0.6Zr (wt pct) samples heat-treated for 16 h at 773 K (500 °C) showing the coexistence of (a) 18R and 14H, and (b) 18R and 24R.

### C. RE-Free Magnesium Alloys with LPSO Structures

A major issue that limits the commercial application of the rare-earth containing Mg alloys is their cost. One avenue to reducing the cost of such alloys would be to utilize misch-metal rather than particular purified rare-earth elements for alloying constituents, and in recent work by Leng *et al.*,<sup>[29]</sup> an Y-rich misch-metal based alloy containing extensive regions of 14H LPSO phase exhibited good strength and ductility: ~300MPa and 27 pct elongation at 523 K (250 °C). However, it would be of significant value to be able to develop RE-free alloys with these same LPSO type structures that offer such excellent strength and ductility properties. There have been several reports of long-period stacking structures in magnesium alloys that do not have any rare-earth alloying elements.<sup>[30-32]</sup> In particular, these structures are found in the Mg-Ni, Mg-Cu-Ni, Mg-Zn-Ni, Mg-Cu-Zn, Mg-Zn-Ag, Mg-Cu-Al, and Mg-Zn-Li systems. However, these long-period structures, ranging from 2 to 21 layers, are quite different from the LPSO structures formed in the RE-containing alloys. Lieser and Witte<sup>[33]</sup> and Komura *et al.*<sup>[30-32]</sup> have shown that the main factor controlling the structural changes in these Friauf-Laves phases is the electron concentration. Further, the structures of these non-rare-earth phases do not contain extended planes of close-packed Mg atoms equivalent to the basal plane of pure magnesium lattice. This is a defining feature of the rare-earth containing LPSO alloys that are all based on multiples of a four-layer building block with the different structures resulting from the number of pure Mg atom layers between

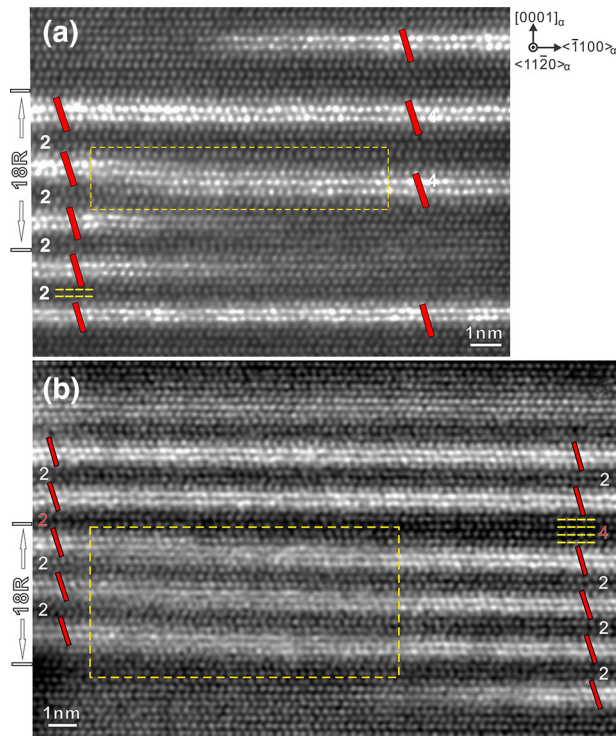


Fig. 7—Atomic-scale HAADF-STEM images in the Mg-8Y-2Zn-0.6Zr (wt pct) samples heat-treated for 1 h at 773 K (500 °C). (a) Shift of one 18R building block and the relocation of Y and Zn atoms result in the appearance of a 24R unit cell; (b) three building blocks of the 18R in left-side shift down together with the relocation of Y and Zn atoms. By this way, the perfect 18R structure is interrupted by a fault arrangement of building blocks with separation distance of 4  $\alpha$ -Mg atomic layers in right side of the image.

each building block. It therefore seems that a key requirement for an Mg alloy to adopt one of the LPSO structures is that the alloying elements are able to form the four-layer ABCA-type building block that provides near perfect matching with the pure Mg hexagonal basal plane.

Characteristically, the Mg-RE based alloys that form the LPSO structures contain a third element, such as Zn, Cu, Ni, or Co, with atomic sizes smaller than Mg, while all of the rare-earth elements have very similar atomic sizes and are larger than Mg. Therefore, in looking for non-rare-earth alloying elements that may produce LPSO structure alloys, a strategy may be to match the atomic radii of the rare-earths. Sc, Na, K, Ca, and Sr all look possible. However, their atomic radii are even larger than the rare-earths, and of course, other atomic characteristics such as electro-negativity may also be a strong influence in the formation and stability of the ordered layers forming the building blocks of the LPSO structures.

### III. TRANSFORMATION OF LPSO PHASES

Both Calphad-type thermodynamic calculations and accumulated experimental observations indicate that the 18R exists as an equilibrium phase in certain alloy

compositions and only at very high temperatures, and that the 14H is an equilibrium phase below 810 K (537 °C).<sup>[21,22]</sup> This implies that the 18R forms directly from the melt during casting of the Mg-Y-Zn alloys, and that the 18R phase will transform into the 14H when the alloys are heat-treated for prolonged periods at relatively low temperatures. The possible phase transformation from 18R to 14H has been observed previously.<sup>[12,13,17,18]</sup> It has been found that the amount of the 14H phase in the intermetallic particles increases with prolonged heat treatment at elevated temperatures. The transformation from the 18R to the 14H involves a change in both structure and composition, and it is therefore in the category of diffusional-displacive transformations.<sup>[34–36]</sup> Figure 6(a) shows the co-existence of 18R and 14H, which proves the possible *in situ* phase transformation of them. However, the co-existence of 18R and 24R has also been observed, Figure 6(b), which indicates that the 24R may be an intermediate phase during the phase transformation from the 18R to the 14H. The evolution process from the 18R to the 14H is usually associated with a specific fault arrangement within the 18R particle—a pair of the ABCA building blocks with a separation distance of 4 atomic layers and the same stacking direction. With the help of this 4-layer fault, the building blocks of the 18R can easily adjust the separation distance to allow a unit cell of 14H to be generated. This process has been named as the “2 + 4” to “3 + 3” transformation mechanism.<sup>[34]</sup> It can be realized by the pair of Shockley partials gliding on two neighboring planes which gives rise to a building block of the 18R shifting upward by one atomic layer and changing its stacking sequence from ABCA to ACBA. With the concomitant shuffle of the Y and Zn atoms, this process leads to a unit cell of the 14H which can grow by the propagation of this ledge. In this situation, the displacive nature of the transformation is dominant with just the short-range movement of the Y and Zn atoms by one atomic layer being required, and no long-range diffusion of Mg atoms is necessary to attain the 14H composition.

Figure 7 shows the atomic-resolution HAADF-STEM images in samples solution treated for 1 hour at 773 K (500 °C). Examination of different areas of the microstructure, Figure 7(a), indicates that the ABCA building blocks are commonly shifted with atomic shuffles. In the left region of the image in Figure 7(a), there are five regularly arranged building blocks separated by 2 close-packed planes of  $\alpha$ -Mg. While the combination of these building blocks could make the 18R structure, the second building block from the top experiences a shift downward by two close-packed atomic layers with atomic shuffles (outlined by the dashed-line rectangle). Through this adjustment, the three building blocks in the top-right side of the image now have separation distance of 4  $\alpha$ -Mg atomic layers. It is of interest to note that the combination of those three blocks in the right side of the image could make a structure unit that has a stacking sequence of ABAB CACACACABCBCBCBACABABA. This stacking sequence is identical to that reported for the 24R structure in the previous work.<sup>[13]</sup>

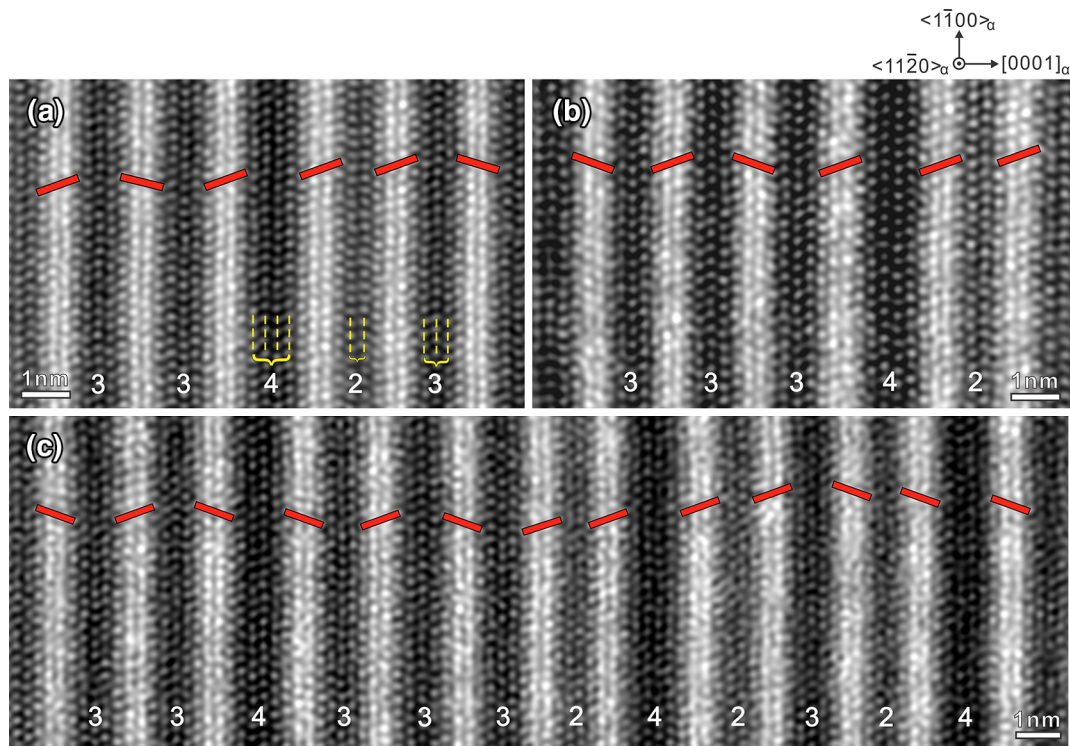


Fig. 8—Atomic-scale HAADF-STEM images in an Mg-8Y-2Zn-0.6Zr (wt pct) sample heat-treated for 1 h at 773 K (500 °C) showing: (a) 14H structure is interrupted by the fault arrangement of the building blocks with the separation distance of 4 and 2 atomic layers; (b) 14H structure associated with the fault arrangement of the building blocks with the separation distance of 4 and 2 atomic layers on right side; and (c) a wide range of fault arrangement of building blocks associated with the 14H. Electron beam is parallel to  $\langle 11\bar{2}0 \rangle_\alpha$ .

Inspection of the image shown in Figure 7(b) reveals that the precipitate in the bottom-left region of the image contains 5 clearly defined building blocks. The separation distance of neighboring building blocks corresponds to 2 close-packed planes of  $\alpha$ -Mg, and thus, they make up the perfect 18R structure. In the bottom-right region of the image, the continuous arrangement of the 18R building blocks is interrupted due to the appearance of a pair of blocks with separation distance of 4  $\alpha$ -Mg atomic layers. This fault arrangement of the building blocks in the 18R structure is generated by moving the three building blocks on the bottom side of the image downward by two atomic layers. Clearly, this process is also associated with additional atomic shuffles\* of Y and Zn atoms (the

\*By shuffles we mean the movement of atoms over just a few atomic distances in contrast to diffusion which involves the long-range movement of atoms.

region in which the atomic shuffles occur is indicated by the dashed-line rectangle). The faulted arrangement provides a basis for the development of the 14H structure *via* the proposed “2 + 4” to “3 + 3” transformation mechanism. It is possible that, during the transformation process from 18R to 14H, the “2” and “4” separations exist in pairs in localized regions for the formation of a perfect 14H structure or exist alone for the formation of an imperfect 14H structure with stacking faults, Figure 8.

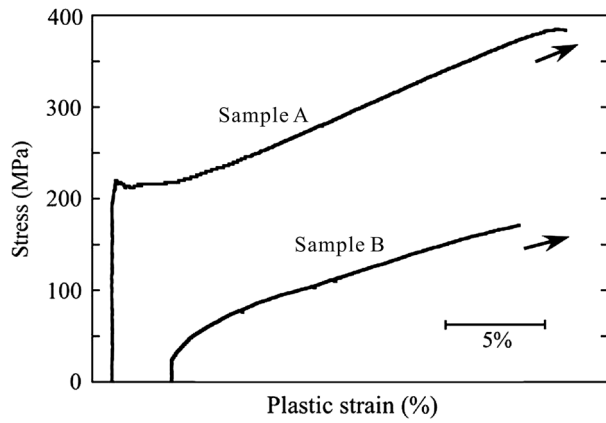
It is also possible to achieve the transformation from the 18R to the 14H without the presence of the stacking

error of the building blocks, but this is considerably more difficult in two ways: (a) without the presence of the 4  $\alpha$ -Mg atomic layer spacing faults between building blocks, the transformation requires long-range diffusion of extra Mg atoms to complete the composition transition, as well as the shuffling of Y and Zn atoms to give the required spacing of the building blocks; and (b) the achievement of the 14H stacking from the 18R stacking requires the coordinated movement of a significant number of Shockley partials with a variety of Burgers vectors to accompany the long-range diffusion and shuffles of Y and Zn atoms.

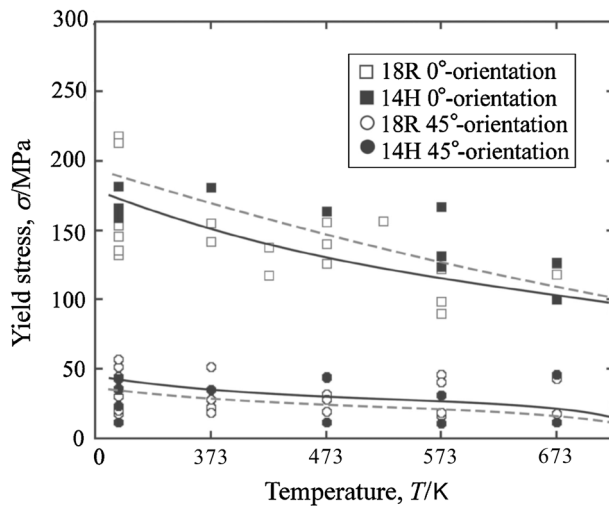
Considering all the LPSO structures reported till now, *i.e.*, 10H, 18R 14H, and 24R with a separation distance of “1”, “2”, “3” and “4,” respectively, one finds that only the combination of “2 + 4” can give rise to “3 + 3” of the 14H, whereas that the combination of “1 + 2” or “1 + 4” cannot result in the appearance of the “3 + 3” structure. Such analysis may explain why the 10H structure is seldom observed in the Mg-Y-Zn alloys. In comparison, regions of the precipitates in which the building blocks are separated by 4 atomic layers and are characteristic of the 24R structure appear frequently to allow a readily transformation to the 14H structure.

#### IV. DEFORMATION MODES OF LPSO PHASES

In developing a detailed understanding of the role of the various LPSO structures in providing the very high strength properties in the Mg-RE-Zn alloys,<sup>[11]</sup> it is



(a)



(b)

Fig. 9—(a) Room temperature compression stress–strain curves for directionally solidified  $\text{Mg}_{12}\text{YZn}$  alloy containing predominantly 18R structure. Sample A orientation: loading direction is parallel to growth direction. Sample B orientation: loading direction is at 45 deg to the growth direction. (b) Variation of yield strength of 18R and 14H structures as a function of testing temperature. (a) and (b) are reproduced from Refs. [38, 39] respectively.

important to understand the deformation characteristics of the LPSO phases themselves, and this has attracted considerable interest in recent years.<sup>[37–41]</sup> Perhaps of greater significance were the extensive studies of the deformation of both the 18R and 14H structures carried out by Hagihara *et al.*<sup>[38–40]</sup> By preparing directionally solidified specimens, they were able to produce very strong growth texture of the LPSO phases, with a  $\langle 11\bar{2}0 \rangle$  direction parallel to the growth direction but with a relatively random orientation perpendicular to the growth direction. Compression tests over a range of temperatures were carried out parallel to and at an angle of 45 deg to the growth direction.

The test results indicated that the  $\text{Mg}_{12}\text{YZn}$  intermetallic alloy with the 18R structure exhibits impressively high plasticity at ambient temperature for tests along both the growth direction and directions at 45 deg to the growth direction, Figure 9(a). For specimens tested with

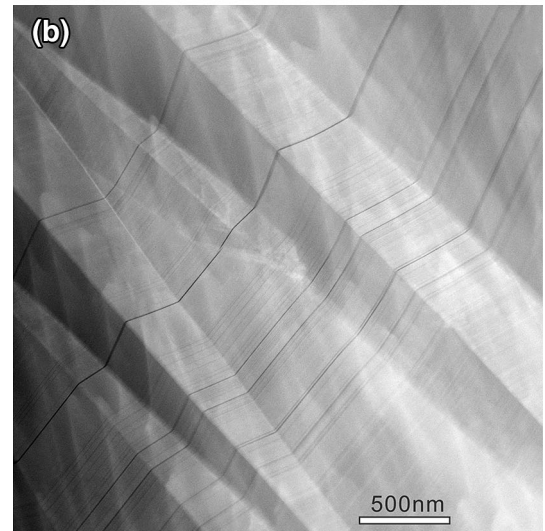
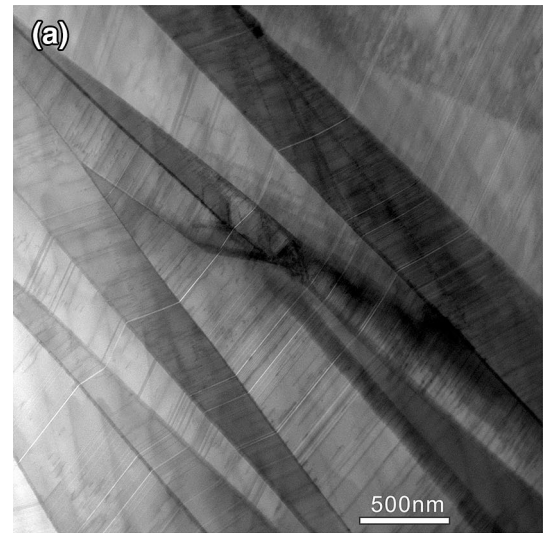


Fig. 10—(a) Bright-field STEM image and (b) HAADF-STEM image showing the kink bands in a deformed Mg-22.4Y-16.5Zn-0.6Zr (wt pct) alloy.

the compression direction at 45 deg to the growth direction, deformation occurred by basal slip, and the yield stress was relatively low at room temperature and decreased further as the temperature increased, Figure 9(b). However, for specimens compressed along the growth direction, *i.e.*, close to a  $\langle 11\bar{2}0 \rangle$  direction, the yield stress was significantly higher and remained high, approximately 100 MPa, even at 673 K (400 °C), Figure 9(b). The key to this remarkable difference in performance is the complete change in the deformation mode between the two orientations. As indicated above, the specimens tested at 45 deg to the growth direction deformed by basal slip. However, for the specimens tested along the growth direction, roughly parallel to  $\langle 11\bar{2}0 \rangle$ , the Schmid factor for basal slip is very low, and deformation took place by the formation of kink bands.<sup>[42–45]</sup> As shown in Figure 10, the kinks produced a local rotation of the lattice with a concomitant shape change. Analysis of electron diffraction patterns indicated that the lattice orientations within the bands were



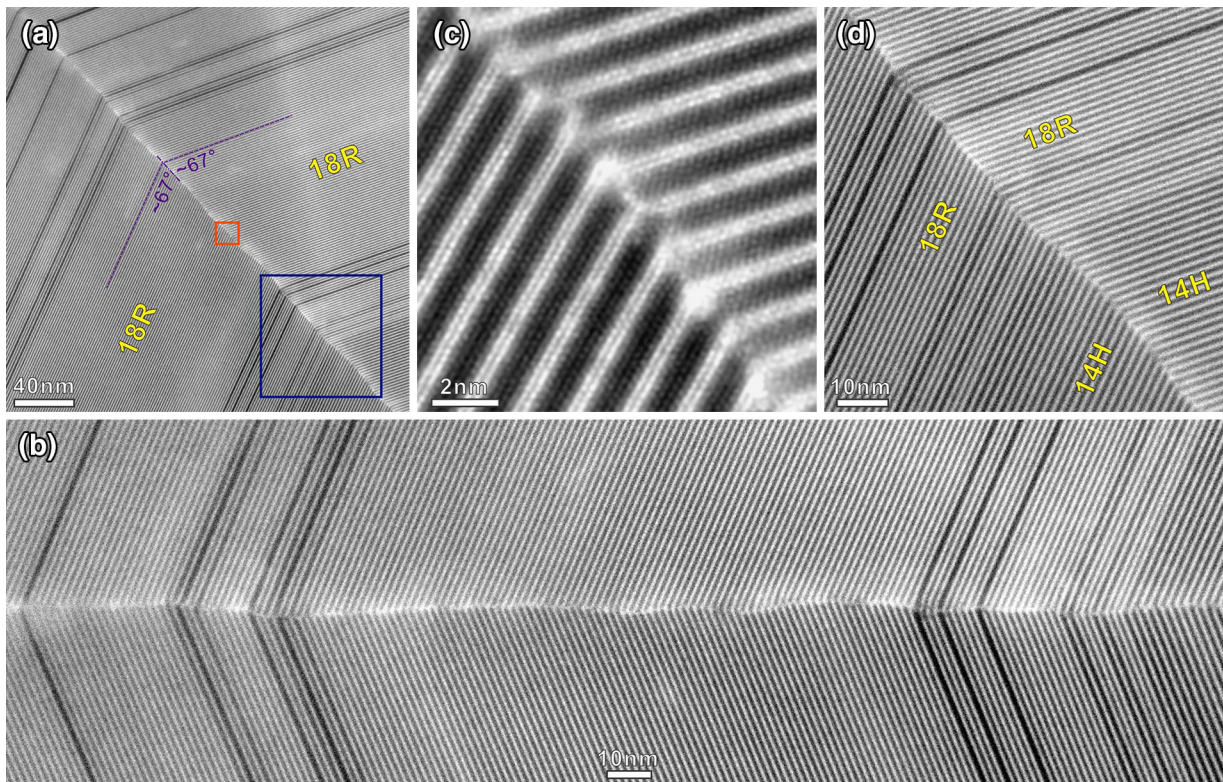


Fig. 11—(a) Low-magnification HAADF-STEM image showing two kink bands and the boundary between them. Most of the regions in the image are associated with the 18R phase; (b) enlargement of the boundary between two kink bands; (c) atomic-scale HAADF-STEM image from the red rectangular frame section in (a); (d) enlargement of the blue rectangular frame section in (a). This image indicates the coexistence of the 18R and 14H, together with some stacking faults.

all close to having a common  $\langle 1\bar{1}00 \rangle$  axis, and dislocations within the kink bands were all of the  $\mathbf{b} = 1/3\langle 11\bar{2}0 \rangle$  type slipping on the basal planes. At the very highest deformation temperatures, non-basal slip was also active in the deformation of high strength ultra-fine grained extruded specimens and was particularly associated with strain accommodation around the kink bands.<sup>[40]</sup>

In a very recent study, Yamasaki *et al.*<sup>[46]</sup> studied extensive kink band formation in an Mg-Zn-Y alloy containing both  $\alpha$ -Mg and 18R LPSO phases, deformed by hot extrusion. The microstructure of the deformed alloy was analyzed using intergranular misorientation analysis (IGMA) based on electron back scattered diffraction (EBSD). It was shown that kink band formation was the major feature of the deformation microstructure in the LPSO phase. Moreover, in this highly constrained deformation mode, four distinct rotation axes describing the kink bands were identified. While the  $\langle 1\bar{1}00 \rangle$  rotation axis was most common, kink bands with rotation axes  $\langle 0001 \rangle$  and  $\langle 1\bar{2}10 \rangle$  were also identified. The IGMA analysis suggested that the dominant slip mode associated with  $\langle 1\bar{1}00 \rangle$  rotation axis was basal slip with prismatic slip, and basal/prismatic slip being required for the  $\langle 0001 \rangle$  and  $\langle 1\bar{2}10 \rangle$  axes, respectively.

With respect to the structure of kink boundary interfaces, optical micrographs (see for example

Figure 12 in Reference 38) and relatively low-magnification TEM images of the kink band interfaces, Figure 10, suggested that the interfaces were highly planar. However, high magnification images reveal that the interfaces are not planar at the atomic level (Figures 11 and 12). The angle between the interface and the close-packed plane is in the range of 67 to 85 deg and in many cases around 70.5 deg, Figure 12(a). Since the angle between the two different close-packed planes in the ABCA building block is  $\sim 70.5$  deg, it would be interesting to examine in the future study whether the atomic plane of the planar interface between the kinks is defined by the near close-packed planes of the 18R or 14H. Equally interesting, the magnitudes of the shear associated with these kinks remain to be established. It is also clear from these observations that the development and propagation of the kink boundaries are not affected by the presence of adjoining regions of 18R and 14H structure, nor of other arrangements of the LPSO type building blocks. This observation is not surprising, since all of the LPSO structures (except 10H) contain pairs, or more, of adjacent hexagonal Mg layers so that basal slip, the major operating mechanism for kink band formation, is readily accommodated. As suggested also by Figure 10, for these strongly textured but polycrystalline specimens deformed under compression, the overall shear component associated with the deformation by kink bands was minimized by the formation of

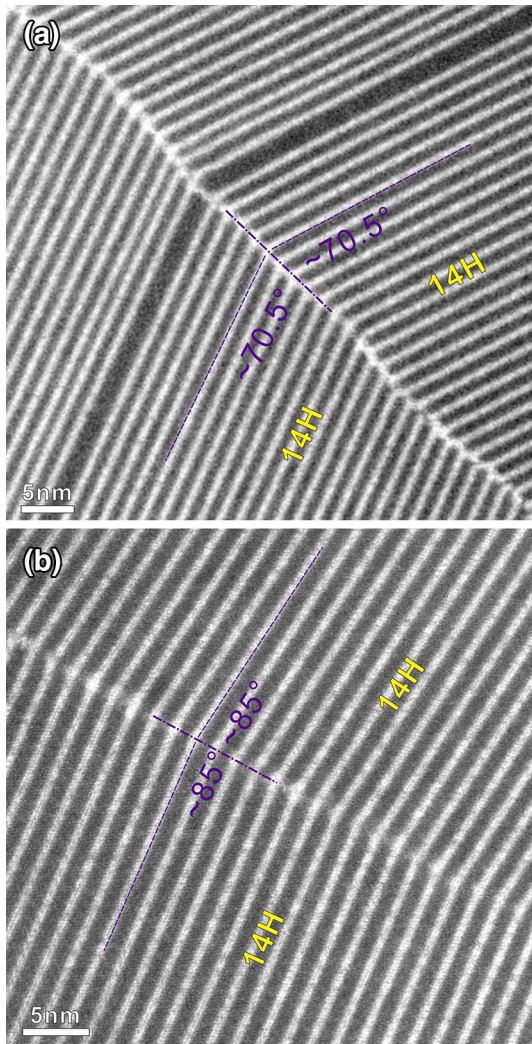


Fig. 12—(a) Low-magnification HAADF-STEM image showing another region of kink bands and their boundary. The bands are comprised 14H phases; (b) Low-magnification HAADF-STEM image showing different tilt angles from (a) between two kink bands across their boundary. The bands are associated with the 14H.

pairs of kink bands with opposing shear directions. This behavior is similar to the formation of self-accommodating martensite plates.

In assessing the nature of the dislocations associated with the kink band formation, Hagihara *et al.*<sup>[38]</sup> concluded that dislocation dipoles were involved. This conclusion was based on their observations of the characteristic shift of dislocation lines in TEM images taken with opposite diffracting vectors,  $\pm\mathbf{g}$ . This result was somewhat surprising since others have found that the component dislocations associated with a particular kink band formation in hexagonal alloys are usually not dislocation dipoles but rather are a pair of basal dislocations with different Burgers vectors. A further analysis of the observations by Hagihara *et al.*<sup>[40]</sup> shows that the dislocation pairs observed may not have been dipoles but were probably composed of dislocations with the two Burgers vectors not parallel to the relevant

diffracting vector, in this case,  $\mathbf{g} = (11\bar{2}0)$ . For example, with a dislocation pair,  $\mathbf{b}_1$  and  $\mathbf{b}_2$ , with Burgers vectors  $1/3[2\bar{1}10]$  and  $1/3[\bar{1}2\bar{1}0]$  respectively, we have

$$\begin{aligned} \mathbf{g} \cdot \mathbf{b}_1 &= 1 & \text{and therefore} & & -\mathbf{g} \cdot \mathbf{b}_1 &= -1 \\ \mathbf{g} \cdot \mathbf{b}_2 &= -1 & \text{and} & & -\mathbf{g} \cdot \mathbf{b}_2 &= 1 \end{aligned}$$

Hence, this pair of dislocations would provide the same image shift characteristics as a dislocation dipole in  $\pm\mathbf{g}$  images taken with the  $(11\bar{2}0)$  diffracting vector.

The fact that the kink formation in the LPSO alloys appears, in the main, to involve the movement of basal dislocations does perhaps provide a significant clue as to the very acceptable ductility of the LPSO phases compared to other intermetallic phases, including the many Mg-based LPS alloys discussed above. The LPSO structures, other than 10H, with their embedded multiple Mg basal plane layers, readily allow basal plane slip without disturbing the ordered building blocks, whereas, for most intermetallic alloys including the non-rare-earth Mg LPS alloys with Friaf-Laves type structures, deformation involves the breaking down of the ordered structure.

It is also worth noting that the very marked difference in strength properties observed with the compression testing parallel to and at 45 deg to the  $\langle 11\bar{2}0 \rangle$  direction for the LPSO phases makes the ability to control the development of texture in the high strength Mg-RE-Zn alloys an important factor in developing maximum properties. It also suggests that the anisotropy between tension and compression behavior, already a feature of magnesium alloys, will be very marked in highly textured materials containing the LPSO phases.

## V. SUMMARY

While LPSO structures formed in Mg-Y-Zn alloys have been studied for a decade, some critical issues on the crystal structure, phase equilibria, transformation, and deformation of LPSO structures still remain unsolved, and considerable efforts are still much needed if these LPSO structures are to be rationally tailored for delivering special mechanical properties. These issues include the following:

1. Is it possible to generate LPSO phases in other alloys systems, particularly in Mg alloys that are free of RE elements? And if so, what are the criteria for the formation of such LPSO phases? The plasticity of Mg-Y-Zn intermetallic alloys appears to be intrinsically good, perhaps due to their unique LPSO structures. A good combination of high strength and acceptable ductility would be expected if the size of the LPSO intermetallics could be significantly refined down to nano-scale by the use of conventional thermomechanical processes. This ultimately raises another question on whether recrystallization can readily occur in these intermetallic alloys when they are plastically deformed to certain strains and, if so, whether the recrystallization occurring during thermomechanical processing or

subsequent annealing can generate ultrafine grains of LPSO structures. It is to be noted that, in very dilute Mg-Y-Zn alloys, e.g., the Mg<sub>97</sub>Y<sub>2</sub>Zn alloy, a yield strength of exceeding 600 MPa together with an elongation to fracture of 6 pct has already been achieved when these alloys are processed by the combined techniques of rapid solidification processing and conventional hot extrusion.

2. While the primary deformation mode of LPSO structure seems to be basal slip, the formation of kinks bands, as the secondary deformation mode, is common. Non-basal slip is also observed to operate to a lesser extent at higher temperatures and under high stress conditions. Kink bands can be treated as a simple shear, but the shear plane and shear direction have not been well defined thus far. Further, the wavy nature of the kink plane at the atomic level suggests that a unique shear plane may not be present. Any progress on this point requires an unambiguous knowledge on the precise structures of LPSO. The conditions for the nucleation of kinks and their growth mechanisms are both unclear. Kinks often form in clusters in deformed samples of Mg-Y-Zn alloys. Each kink has a spearhead morphology resembling that of some martensites. The interfaces of these kinks are planar at the micron scale but wavy at the nano- or atomic-scale. The strain associated with the formation of such kinks, and its relation to the overall plastic deformation of the alloy, has not been well characterized and analyzed. Similarly, the shear strain and therefore the shape change associated with these kinks have not been defined either. It remains to be established whether these kinks form in pairs and back-to-back, i.e., with opposite shears to minimize the strain, although the observation of groups of mini-kinks may throw some light on this issue.

## ACKNOWLEDGMENTS

The authors acknowledge gratefully the financial support from the Australian Research Council, the access to the facilities of the Monash Centre for Electron Microscopy and Yangxin Li and Ruiqi Chen for sample preparation.

## REFERENCES

1. Z.P. Luo, S.Q. Zhang, Y.L. Tang, and D.S. Zhao: *J. Alloys Compd.*, 1994, vol. 209, pp. 275–78.
2. M. Yamasaki, T. Anan, S. Yoshimoto, and Y. Kawamura: *Scripta Mater.*, 2005, vol. 53, pp. 799–803.
3. M. Yamasaki, M. Sasaki, M. Nishijima, K. Hiraga, and Y. Kawamura: *Acta Mater.*, 2007, vol. 55, pp. 6798–805.
4. J.F. Nie, K. Oh-ishi, X. Gao, and K. Hono: *Acta Mater.*, 2008, vol. 56, pp. 6061–76.
5. K. Yamada, Y. Okubo, M. Shiono, H. Watanabe, S. Kamado, and S. Kojima: *Mater. Trans.*, 2006, vol. 47, pp. 1066–70.
6. K. Amiya, T. Ohsuna, and A. Inoue: *Mater. Trans.*, 2003, vol. 44, pp. 2151–56.

7. M. Matsuura, K. Konno, M. Yoshida, M. Nishijima, and K. Hiraga: *Mater. Trans.*, 2006, vol. 47, pp. 1264–67.
8. S.B. Mi and Q.Q. Jin: *Scripta Mater.*, 2013, vol. 68, pp. 635–38.
9. E.M. Padezhnova, E.V. Melnik, R.A. Milyevskiy, T.V. Dobatkina, and V.V. Kinzhbalov: *Russ. Metall. (Engl. Transl.)*, 1982, vol. 4, pp. 185–88.
10. Z.P. Luo and S.Q. Zhang: *J. Mater. Sci. Lett.*, 2000, vol. 19, pp. 813–15.
11. Y. Kawamura, K. Hayashi, A. Inoue, and T. Masumoto: *Mater. Trans.*, 2001, vol. 42, pp. 1172–76.
12. T. Itoi, T. Seimiya, Y. Kawamura, and M. Hirohashi: *Scripta Mater.*, 2004, vol. 51, pp. 107–11.
13. M. Matsuda, S. Ii, Y. Kawamura, Y. Ikuhara, and M. Nishida: *Mater. Sci. Eng. A*, 2005, vol. 393, pp. 269–74.
14. E. Abe, Y. Kawamura, K. Hayashi, and A. Inoue: *Acta Mater.*, 2002, vol. 50, pp. 3845–57.
15. D.H. Ping, K. Hono, Y. Kawamura, and A. Inoue: *Philos. Mag. Lett.*, 2002, vol. 82, pp. 543–51.
16. Y.M. Zhu, A.J. Morton, and J.F. Nie: *Acta Mater.*, 2010, vol. 58, pp. 2936–47.
17. S. Yoshimoto, M. Yamasaki, and Y. Kawamura: *Mater. Trans.*, 2006, vol. 47, pp. 959–65.
18. J. Lee, K. Sato, T.J. Konno, and K. Hiraga: *Mater. Trans.*, 2009, vol. 50, pp. 222–25.
19. A. Ono, E. Abe, T. Itoi, M. Hirohashi, M. Yamasaki, and Y. Kawamura: *Mater. Trans.*, 2008, vol. 49, pp. 990–94.
20. J. Grobner, A. Kozlov, X.Y. Fang, J. Geng, J.F. Nie, and R. Schmid-Fetzer: *Acta Mater.*, 2012, vol. 60, pp. 5948–62.
21. J.F. Nie: *Metall. Mater. Trans. A*, 2012, vol. 43A, pp. 3891–939.
22. Y.M. Zhu, M. Wayland, A.J. Morton, K. Oh-ishi, K. Hono, and J.F. Nie: *Scripta Mater.*, 2009, vol. 60, pp. 980–83.
23. H. Yokobayashi, K. Kishida, H. Inui, M. Yamasaki, and Y. Kawamura: *Acta Mater.*, 2011, vol. 59, pp. 7287–99.
24. D. Egusa and E. Abe: *Acta Mater.*, 2012, vol. 60, pp. 166–78.
25. J.E. Saal and C. Wolverton: *Scripta Mater.*, 2012, vol. 67, pp. 798–801.
26. H. Kimizuka, M. Fronzi, and S. Ogata: *Scripta Mater.*, 2013, vol. 69, pp. 594–97.
27. K. Kishida, H. Yokobayashi, and H. Inui: *Philos. Mag.*, 2013, vol. 93, pp. 2826–46.
28. E. Abe, A. Ono, T. Itoi, M. Yamasaki, and Y. Kawamura: *Philos. Mag. Lett.*, 2011, vol. 91, pp. 690–96.
29. Z. Leng, J.H. Zhang, M.L. Zhang, X.H. Liu, H.B. Zhan, and R.Z. Wu: *Mater. Sci. Eng. A*, 2012, vol. 540, pp. 38–45.
30. Y. Komura, M. Mitarai, I. Nakatani, H. Iba, and T. Shimizu: *Acta Cryst.*, 1970, vol. B26, pp. 666–68.
31. Y. Komura, A. Nakaue, and M. Mitarai: *Acta Cryst.*, 1972, vol. B28, pp. 727–32.
32. Y. Komura and Y. Kitano: *Acta Cryst.*, 1977, vol. B33, pp. 2496–501.
33. K.H. Lieser and H. Witte: *Z. Metall.*, 1952, vol. 43, pp. 396–401.
34. Y.M. Zhu, A.J. Morton, and J.F. Nie: *Acta Mater.*, 2012, vol. 60, pp. 6562–72.
35. T. Kiguchi, Y. Ninomiya, K. Shimmi, K. Sato, and T.J. Konno: *Mater. Trans.*, 2013, vol. 54, pp. 668–74.
36. T. Furuhashi and X.F. Gu: *Mater. Trans.*, 2013, vol. 54, pp. 668–74.
37. X.H. Shao, Z.Q. Yang, and X.L. Ma: *Acta Mater.*, 2010, vol. 58, pp. 4760–71.
38. K. Hagihara, N. Yokotani, and Y. Umakoshi: *Intermetallics*, 2010, vol. 18, pp. 267–76.
39. K. Hagihara, Y. Sugino, Y. Fukusumi, Y. Umakoshi, and T. Nakano: *Mater. Trans.*, 2011, vol. 52, pp. 1096–103.
40. K. Hagihara, Y. Fukusumi, M. Yamasaki, T. Nakano, and Y. Kawamura: *Mater. Trans.*, 2013, vol. 54, pp. 693–97.
41. E. Onorbe, G. Garces, P. Perez, and P. Adeva: *J. Mater. Sci.*, 2012, vol. 47, pp. 1085–93.
42. E. Orowan: *Nature*, 1942, vol. 149, pp. 643–44.
43. B. Hess and C.S. Barrett: *Trans. Am. Inst. Min. Met. Eng.*, 1949, vol. 185, pp. 599–606.
44. A.G. Crocker and J.S. Abell: *Philos. Mag.*, 1976, vol. 33, pp. 305–10.
45. L. Farber, I. Levin, and M.W. Barsoum: *Philos. Mag. Lett.*, 1999, vol. 79, pp. 163–70.
46. M. Yamasaki, K. Hagihara, S. Inoue, J.P. Hadorn, and Y. Kawamura: *Acta Mater.*, 2013, vol. 61, pp. 2065–76.